A small key unlocks a heavy door:
The essential function of the small hydrophobic proteins SP-B and SP-C to trigger adsorption of pulmonary surfactant lamellar bodies

Nina Hobi [1,2,#], Michael Giolai [1], Bárbara Olmeda [2], Pika Miklavc [1], Edward Felder [1], Paul Walther [4], Paul Dietl [1], Manfred Frick [1], Jesus Pérez Gil [2§] and Thomas Haller [b,§]

[1] Institute of General Physiology,
Ulm University, Albert-Einstein Allee 11, 89081 Ulm, Germany.

[2] Department of Physiology and Medical Physics, Division of Physiology,
Medical University of Innsbruck, Fritz-Pregl-Str. 3, A-6020 Innsbruck, Austria.

[3] Departamento de Bioquimica y Biologia Molecular, Facultad de Biologia, and Research Institute Hospital 12 Octubre,
Universidad Complutense, José Antonio Novais 2, 28040 Madrid, Spain

[4] Central Facility for Electron Microscopy,
Ulm University, Albert-Einstein-Allee 11, 89081 Ulm.

[#]Corresponding author:
Nina Hobi
Institute of General Physiology
University of Ulm
Albert-Einstein-Allee 11
89081 Ulm
Germany
Tel. 0731 500-23231
Fax 0731 500-23242
E-mail: Nina.Hobi@uni-ulm.de

[$]shared senior authors

Key words: ARDS, compliance, lamellar-body, lung injury, surface tension

Abstract

The molecular basis involving adsorption of pulmonary surfactant at the respiratory air-liquid interface (A_{LI}) and the specific roles of the surfactant proteins SP-B and SP-C in this process have not been completely resolved. The reasons might be found in the largely unknown structural assembly in which surfactant lipids and proteins are released from alveolar type II cells, and the difficulties to sample, manipulate and visualize the adsorption of these micron-sized particles at an A_{LI} under appropriate physiological conditions. Here, we introduce several approaches to overcome these problems. First, by immunofluorescence we could demonstrate the presence of SP-B and SP-C on the surface of exocytosed surfactant particles. Second, by sampling the released particles and probing their adsorptive capacity we could demonstrate a remarkably high rate of interfacial adsorption whose rate and extent was dramatically affected by treatment with antibodies against SP-B and SP-C. The effect of both antibodies was additive and specific. Third, direct microscopy of an inverted A_{LI} revealed that the blocking effect is due to a stabilization of the released particles when contacting the A_{LI}, precluding their transformation and the formation of surface films. We conclude that SP-B and SP-C are acting as essential, preformed molecular keys in the initial stages of surfactant unpacking and surface film formation. We further propose that surfactant activation might be transduced by a conformational change of the surfactant proteins upon contact with surface forces acting on the A_{LI}.

Introduction

Pulmonary surfactant is a surface active lipoprotein complex synthesized by the alveolar type II (AT II) cells. It is stored in special organelles, the lamellar bodies (LBs), probably in the form of tightly packed lipid bilayers in small repeat distances (Ochs, 2010). Upon stimulation of AT II cells, this dense lipoprotein-complex is released into the thin alveolar lining fluid (Bastacky et al., 1995) by constitutive and regulated exocytosis (Dietl and Haller, 2005;Frick et al., 2001) and in an active squeeze-out process through a constricted fusion pore (Miklavc et al., 2012). After secretion, the surfactant complexes are essentially stable in the aqueous milieu even demonstrating considerable viscoelastic properties (Singer et al., 2003). They maintain this particulate, spherical structure (= lamellar body like particles, LBPs; (Ravasio et al., 2010)) until contact with a clean air-liquid interface (A_{LI}), where LBPs (Ø 1-5 µm) spontaneously and rapidly disintegrate to deliver surface active materials into the expanding surface film (Ravasio et al., 2010;Hobi et al., 2014;Haller et al., 2004;Bertocchi et al., 2005). Evidence is growing that LBPs constitute the most original form in which surfactant is exocytosed by the AT II cells, and tubular myelin is suggested as a secondary, but not obligatory, form feeding directly into a growing surface film (Perez-Gil, 2008).

The major fraction of pulmonary surfactant is composed of lipids, predominantly saturated phospholipids like dipalmitoylphosphatodylcholine (DPPC) and a minor fraction of neutral lipids such as cholesterol. The specific phospholipid composition, in particular the high amount of DPPC, makes surfactant a biologically unique membrane system able to sustain high surface pressures and thus to maintain a very low surface tension (γ) upon lateral compression. However, the stiff nature of DPPC compromises the flexibility and the dynamics of the interfacial structures. These properties, which are of critical importance during the respiratory cycle, are assured by the hydrophobic surfactant proteins B and C (Perez-Gil, 2008).

SP-B, a 79-residue polypeptide belonging to the saposin-like protein family (Parra et al., 2013) has a molecular weight of 8.7 kDa and preferably forms a covalent homodimer of 19 kDa, which is the most abundant protein configuration found in surfactant membranes (Hawgood et al., 1998;Perez-Gil, 2008). Due to its high hydrophobicity SP-B is permanently membrane-associated and it primarily interacts with anionic phospholipids like phosphatidylglycerol (PG) (Cabre et al., 2012;Perez-Gil et al., 1995). Its amphipathic character and the presence of charged residues suggest a superficial interaction of SP-B with both bilayers and monolayers. SP-B binds to phospholipid membranes, promotes membrane-membrane contacts (Cabre et al., 2009) causes lipid fusion, and

contributes to the formation of multilayer lipid structures (Bernardino et al., 2013). Interestingly, SP-B has a strong tendency to form large oligomers in bi- and monolayers, probably forming large hydrophobic pores (Olmeda et al., 2015). Furthermore, SP-B also plays a critical role in the intracellular biogenesis of surfactant, being required for the proper formation of LBs and the proteolytic processing of SP-C (Stahlman et al., 2000). The absolutely decisive function and clinical relevance of SP-B is undoubted, since several studies describe that a complete lack of SP-B in newborn mice and humans cause lethal respiratory failure at birth (Clark et al., 1995;Melton et al., 2003;Tokieda et al., 1997;Weaver and Beck, 1999). SP-C, a small lipopeptide of 4.5 kDa with 35 residues, is exclusively produced in lungs by the AT II cells. Its amino acid sequence includes in most species two neighboring cysteines which are palmitoylated. This post-translational modification confers a tight association of the protein N-terminal segment with bilayers and interfacial films, thereby preventing its exclusion from the interface during compression (Lukovic et al., 2012;Plasencia et al., 2001). Thus, SP-C is believed to promote and stabilize membrane-interface contacts and to facilitate lipid exchange between lipid layers (Glasser et al., 2001;Lukovic et al., 2012). In contrast to SP-B, SP-C is not as absolutely essential for lung ventilation and survival. However, SP-C deficient mice ultimately develop chronic respiratory failure (Glasser et al., 2008;Lawson et al., 2005). Although SP-B and SP-C possess a very different molecular structure, they are both lipid membrane associated and thus probably perform their surface activity in a concerted manner. Together they improve surfactant activity, in particular interfacial adsorption, film stability and its re-spreading abilities (Cruz et al., 2000;Serrano and Perez-Gil, 2006;Wang et al., 1996) and it has been shown that these roles are particularly relevant at extensive lung expansion and relaxation during periods of high ventilatory demands (Almlen et al., 2008).

It has been argued that surfactant in its original, compact and lamellated structure is not able to adsorb at the A_{LI} directly and, consequently, needs to be ‘activated’. Theories on the kind of activation focused on an enzymatic cleavage process (convertase) in combination with exposure of LBPs to mechanical forces acting at the A_{LI} (Gross and Schultz, 1990) and a Ca^{2+}/SP-A promoted unraveling and rearrangement of the surfactant PL-bilayers into a three-dimensional lattice structure (tubular myelin) feeding single PL molecules into an expanding film (Gil and Reiss, 1973). According to another hypothesis, surfactant is activated by the deformation during its passage through the fusion pores (Kliewer et al., 1985). Up to now, however, an experimental proof of either concept is still missing. We instead propose that LBPs are structurally pre-assembled in a way that enables a direct and rapid adsorption at an A_{LI} in the absence of any metabolic or structural intermediate. Upon surface contact, the small hydrophobic surfactant proteins SP-B and SP-C are

acting, probably in concert and probably on the outermost surfactant lipid layer, as a molecular trigger to unravel the compact LBP structure and to initiate the initial stage of surface film formation. This model also implies a decisive role of interfacial tension as the essential driving force in this process**.**

Results and Discussion

Characterization of AT II cells and collected LBPs

As demonstrated by confocal microscopy, primary cultures of AT II cells, grown for 48h on plastic, exhibit a typical morphology. They contain a large number of surfactant storage vesicles (=LBs), which are stained by fluorescence targeted against the ATP-binding cassette transporter A3 (ABCa3), a specific LB membrane marker (Fig. 1, red) (Yamano et al., 2001). As indicated with arrows, intracellular LBs contain substantial amounts of surfactant proteins SP-B and SP-C. Both proteins show a particular granule-like packing (Fig. 1, green), which is bordered by the vesicle's limiting membrane (Fig. 1, red). To our knowledge, this is the first demonstration of the distribution of SP-B and SP-C in LBs of primary ATII cells using high resolution confocal microscopy.

Highly pure ATII cell cultures were stimulated with a solution containing 100µM ATP + 300nM PMA. Thereafter, cell supernatants containing released LBPs in suspension were harvested and immediately frozen at -20°C. The PL concentration of the collected samples was evaluated as previously described (Hobi et al., 2014;Ravasio et al., 2008;Ravasio et al., 2010). Western Blots (n=3) were performed under non reducing conditions. As shown in Fig. 2. the collected samples contain significant amounts of SP-B and SP-C. Detected band sizes are comparable to samples from rat bronchoalveolar lavage (BAL), serving as a positive control. *In vivo* the amount of SP-B and SP-C is very small, indeed less than one percent of the entire surfactant mass. This small fraction, though, plays a crucial role in surfactant function (Casals, 2001;Serrano and Perez-Gil, 2006). In summary, we suggest that with respect to the molecular content and lipid packaging, freshly collected LBPs are the most original and authentic source of pulmonary surfactant currently used for surfactant studies.

Localization of the hydrophobic surfactant proteins

We analyzed immunofluorescence of the hydrophobic surfactant proteins on cell-attached LBPs. In this transitional state, which is neither purely intra- nor extracellular, LBPs are partially exposed to the extracellular fluid and partially trapped by a restricted diameter of the exocytotic fusion pore

(Haller et al., 2001). Thus, in a sense, LBPs are mechanically arrested and can be used for detailed microscopic investigations. To activate exocytosis, AT II cells have been stimulated with 100µM ATP for 15 min (Haller et al., 2001). Subsequently, the cells have been washed and exposed with primary rabbit anti SP-B (aSPB) or rabbit anti SP-C (aSPC) and finally with secondary anti rabbit Alexa488 conjugated antibody. All stainings were done on living cells, under cold conditions to prevent unspecific binding or intracellular antibody (AB) uptake by endocytosis. First, cell attached LBPs were identified by a 2 min time lapse protocol using transmitted light (Fig. 3, 1th and 2nd column, BF). LBPs that protrude out of fused LBs are noticeable by irregular movements of their extracellular portion (Haller et al., 2001). In parallel, AB staining was recorded by exciting Alexa488 fluorescence (Fig 3, 4th column, aSPB and aSPC). Thereafter cells were additionally stained with extracellular FM1-43, a lipid membrane probe well documented to be suited for staining cell attached LBPs (Fig. 3, 3rd column, FM 1-43) (Haller et al., 1998). Examples for cell attached LBPs are indicated with blue arrows. Negative controls, lacking primary ABs, proved the specific binding of the applied ABs (Fig. 3, n.c., Movie S1_neg.ctrl). Images show a specific antigen staining of SP-B and SP-C in freshly released but still plasma membrane-attached LBPs (Fig. 3 aSPB and aSPC; Movie S2_SPB and Movie S3_SPC). In summary these findings demonstrate that, immediately after LB fusion and onset of LBP release, SP-B and SP-C epitopes are freely accessible to the antibodies from the extracellular side. This can be taken as a first evidence of a peripheral location of the two proteins on LBPs.

By using scanning electron microscopy (SEM) we aimed at a closeup of the LBPs surface and the specific protein location. Partially extruded LBPs in the same transitional state as above were stained with aSPB and aSPC followed by an immunogold (25 nm) labeling. As shown in Fig. 4, LBPs stay in compact, ballon-like aggregates during release. Gold particles were visualized with backscattered electrons (Fig. 4 right) and specifically target SP-B on the outmost LBP membrane protrusions (inset and arrows). Upon now, few EM studies exist focusing on SP localization. By using immune-TEM, Brasch et al. described that in human cells SP-B is restricted to a so-called projection core, a peripheral structure of randomly arranged stacks of densely packed membrane segments (Brasch et al., 2004). This finding has been confirmed by Ochs et al. in 2010 using a combination of in-situ fixation, cryopreparation and colloidal gold immuno-TEM (Ochs, 2010). Interestingly, in LBs of rat lungs, lacking such a projection core, SP-B was more evenly distributed over the lamellae (Brasch et al., 2004) and similar observations exist for the mouse (Liou et al., 1996). Despite these supportive results, these TEM studies do not allow to conclude that SP-B is also located at the external face of

extruded LBPs. To our knowledge, this is the first demonstration of surface localization of SP-B in fully intact LBPs.

In contrast, immunogold staining failed to detect SP-C despite several experimental replicates. However, this finding would be consistent with recent data on SP-C location and orientation in lipid-bilayers (Pastrana et al., 1991;Vandenbussche et al., 1992). These studies describe that the monomeric SP-C molecule is completely inserted into the membrane interior except for the N-terminal residue, which barley projects from the strongly negatively charged lipid surface (Roldan et al., 2015;Vandenbussche et al., 1992). In comparison, native SP-B is more positively charged than SP-C, and SP-B was recently modelled to build huge complexes up to 10nm, which significantly protrude out of the plane of the lipid layers (Olmeda et al., 2015). It has been proposed that SP-B/SP-C complexes form pores in surfactant membranes that are smaller than those formed by SP-B alone (Parra et al., 2013). It is therefore also conceivable that bare antibodies are small enough to get access to SP-C but not once they are conjugated to bulge gold particles.

Functional SP-B and SP-C are critical for rapid interfacial adsorption of LBPs

Few years ago, our lab developed a method for measuring phospholipid surface film formation in the fluorescence mode of a multiplate reader instrument (Ravasio et al., 2008). In comparison to conventional techniques such as Langumir-Whilhemy surface balance and captive bubble surfactometry, this assay allows simultaneous kinetic analysis of the extremely low surfactant quantities (ng range) with which we are confronted in this study (Danhaive et al., 2015;Hobi et al., 2014;Ravasio et al., 2008). Here, we used this assay to test whether blockage of SP-B or SP-C with rabbit aSPB or aSPC leads to a substantial change in LBPs adsorption. For that we prepared different AB solutions in a concentration range between 2 to 100 nM. First we measured the transparent control and tested if ABs affect Bodipy-PC fluorescence. This was not the case (Fig. 1S, Inset). Furthermore, we used rabbit anti-IgG (aIgG) to verify possible surface interactions of the ABs by themselves. In line with recent publications (Danhaive et al., 2015;Hobi et al., 2014), we defined the maximum fluorescence value, which reflects the steady state surfactant film formation after maximal adsorption, as *Max*. Additionally, we calculated the *Slope* (=ΔRFU/min) of the initial adsorption, which is a critical parameter to evaluate the adsorption dynamics (Fig. S1). As shown in Fig. 5A, a 100nM aSPB (n=6) or aSPC (n=6) solution had a dramatic effect on adsorption kinetics and surfactant film formation (*Kinetics*) of freshly collected LBPs. Blockage of either protein therefore seem to prevent rapid initial adsorption to reach highest *Max* (Fig. 5B and C, *P*<0.05, P**<0.01, P***<0.001*). Furthermore, already very low AB concentrations (10nM and 20nM) showed a small tendency of *Max* inhibition (Fig. 5B) and a significant reduction of the initial slope (Fig. 5C). The

results are consistent with studies describing that both, SP-B and SP-C, promote lipid adsorption at the A_{LI}. Moreover, it is suggested that these two proteins might have a combined or even synergistic function for optimal surface activity (Klenz et al., 2008;Parra and Perez-Gil, 2015;Schürch et al., 2010). We tested this hypothesis by adding aSPB and aSPC simultaneously. The result was a highly significant and dose-dependent functional loss of LBPs (Fig. 5 SP-B + SP-C, n=10-14). *Max* and *Slope* of aSPB+C treated samples were significantly reduced in comparison to the negative controls (aIgG and w/o). Furthermore, regarding *Max*, a combined application of aSPB+C (2-20nM) showed a strong and highly significant reduction in comparison to aSPB or aSPC alone (indicated with $P^{\#}$<0.05, $P^{\#\#}$<0.01, $P^{\#\#\#}$<0.001 against SPB (B) and SPC (C)). In comparison with previous studies, these results confirm that SP-B and SP-C are both important for rapid and maximal surfactant adsorption. We found that the functional loss of one protein might still permit partial activity by the other protein, suggesting that the two proteins might not only act in an additive but even in a cooperative way. This interplay is apparently less important for the initial phase of LBPs adsorption (Fig. 5 *Slope*) than for reaching highest adsorption capacity (Fig.5 *Max*). Recently, the same adsorption assay was used to distinguish the film formation properties of therapeutically used surfactants, and it was noted that the amount of SP-B in the samples critically affects surfactant film formation. The amount of SP-C, however, was not tested in these studies. Furthermore, adding SP-B and SP-C into extracted phospholipids from healthy infant resulted in an additive 6–fold increase in *Max* (Danhaive et al., 2015).

Blockage of hydrophobic surfactant protein directs LBPs inactivation

We previously demonstrated by the inverted interface microscopy (Haller et al., 2004;Hobi et al., 2012;Ravasio et al., 2010) that freshly released LBPs spontaneously and rapidly disintegrate when they contact the A_{LI}, creating an interfacial film with a solid character and a three-dimensional complex topography (Haller et al., 2004;Ravasio et al., 2010). Importantly, the high γ at a clean interface (γ = 72mN/m) was the driving force for LBP transformation, and it constantly decreased to values ~30 mN/m with the continued incorporation of new material (Bertocchi et al., 2005;Haller et al., 2004). Hence, as the driving force for LBPs adsorption ceased, LBPs remained untransformed and clustered beneath the A_{LI}.

In this study we used the inverted interface technique to investigate LBPs transformation in the presence of the respective blocking ABs. We have summarized the critical steps of the experimental protocol in Fig. 6 and refer for a detailed explanation to previous publications (Bertocchi et al., 2005;Haller et al., 2004;Ravasio et al., 2011). Fig. 6A sketches the heated chamber filled with

experimental solution. FM1-43 preloaded LBPs were gently pipetted into that solution and reach the A_{LI} by slow sedimentation. Upon random interface contact (Bertocchi et al., 2005;Haller et al., 2004;Ravasio et al., 2010) LBPs spontaneously disintegrate (=transform, Fig. 6B; Movie S4A and S4B) and spread into a surface film (Ravasio et al., 2010). Here, we investigated these events in the presence of aSPB and/or aSPC by using two different approaches. In the first one (protocol A), we filled the pre-heated chamber with bath solution (37 °C) containing different concentrations of aSPB and aSPC (2nM-100nM). Subsequently, FM 1-43 loaded LBPs were added. To disclose a possible interfacial effect of unbound AB, we pre-incubated LBPs with ABs (1µM to 20nM for 2h) and removed unbound ABs by a repeated, careful washing before adding them to the chamber (protocol B). In both protocols we used untreated LBPs (w/o) and anti-rabbit IgG (aIgG) in the equivalent concentrations as a negative control. The sedimentation curves of Fig. 6C are representative for the total number of LBPs that arrived at the interface during the first 10 min. No significant difference could be observed between protocol A (52±2, n=20) and protocol B (50±2, n=20). Also, AB treatment had no effect on the sedimentation rates or the shape/size of the LBPs.

The analysis of LBP transformation is shown in Fig. 7. When using protocol A, LBPs showed an average transformation rate of 19 ± 3 (w/o, n=11) or 20 ± 2 (100nM aIgG, n=17) under control conditions. Presence of aSPB or aSPC, even in the smallest concentrations (2nM), lead to a very strong inhibition and dose-dependent effect on the transformation rate at the A_{LI} (Fig. 7A; n=10-15). Furthermore, we also tested aSPB and aSPC together. The effect was a cumulative one. In comparison to the individual application of aSPB or aSPC in small amounts from 2nM-20nM, the combined application (aSPB+C) resulted in a more than 50% decline of LBPs adsorption (Fig. 7A; aSPB+C, n=10). These microscopic data are consistent with the quantitative data performed with the adsorption assay in Fig. 5.

In protocol B (Fig. 7B), LBPs without AB (w/o) or incubated with 1µM aIgG showed a mean disintegration of 23±2 LBPs or 20±1 LBPs within 10 min, respectively. Treatment with 1µM aSPB or aSPC significantly reduced transformation rate to less than 5±2 LBPs. Less AB concentrations between 10-100nM had a smaller but still significant effect (Fig. 7B, n=10-12). Similar as in previous experiments, the combined application of both ABs (aSPB+C) lead to a further reduction of LBP adsorption. In particular, treatment with 10nM aSPB+C lead to a transformation rate of 5±1 LBPs in comparison to 13±2 LBPs (n=10) and 20 ±2 LBPs (n=10) by using aSPB and aSPC individually. Both protocols lead to highly comparable results. The slightly weaker effect in protocol B could be explained by antibody washout leaving some epitopes unaffected. Even more likely, during surface contact and beginning particle disintegration, additional epitopes could become accessible, particularly those in SP-C, which cannot be blocked using protocol B.

Many studies described a surface activity of highly concentrated protein and AB solutions by themselves, a factor that could potentially confound our interpretations (Holm et al., 1985;Mahler et al., 2009;Taeusch et al., 2005;Zasadzinski et al., 2005). However, the AB concentration used in our first approach (Protocol A, 2nM-100nM) was much lower, than the concentrations reported to cause a significant effect on surface pressure (Herting et al., 1999;Mahler et al., 2009;Taeusch et al., 2005). By pre-treatment of LBPs with AB followed by washout of unbound AB (Protocol B) we can rule out this possibility almost entirely. Furthermore, we also used IgG as a negative control in the same concentration as aSPB and aSPC without observing an effect. Finally, the additive effect of aSPB and aSPC strongly suggests a specific interaction of the ABs with the LPBs surface.

Change in local surface pressure reflected by LBPs motility

The unpacking of LBPs, whether caused by physical, chemical or other factors, is an essential prerequisite for lipid insertion into the A_{LI}. Probably the most striking of these events is the immediate loss of LBP structure when they contact an A_{LI}, delivering a bulk of material into small surfaces patches. We observed that during these patch formations, all other discernable surface structures, including non-adsorbed and only partially transformed LBPs, are subject to rapid lateral motions and hypothesize that they are due to a liquid flow generated by local surface pressure (tension) gradients (Marangoni-effects). This is evidenced by the second observation that the mean velocity of particle movement gradually ceased with ongoing LBP conversions and eventually comes to a halt when γ- gradients are abolished, after formation of a continuous film (Bertocchi et al., 2005). In that case, like in a pure surfactant-free solution, the velocity of fluorescent beads embedded onto our inverted A_{LI}, turned out to be zero (Ravasio et al., 2010). Therefore, we exploited this phenomenon as a probably very sensitive indicator for the insertion of surface active material out of transformed LBPs. Lateral particle mobility was measured and traced by a semi-automated 2/3D single-particle tracking tool from the mosaic group (Sbalzarini and Koumoutsakos, 2005). The program detects all spot-like surface structures of a defined cut-off for fluorescence intensity and pixel size (see Fig. 8, A-C and Movie S5). As shown in control conditions, lateral velocity (µm/sec) is high during the first 10 initial LBPs adsorption events (0.67µm/sec, n=4 representative tracks) and slowed down, with an exponential decay, to 0.35 µm/sec during further LBP adsorption (Spearman's correlation coefficient = -0.93; $P < 0.0001$, Fig. 8C). As shown in Fig. 8D, when using protocol B the average particle velocity within the first 10 min was 62 ± 3 µm for control LBPs (w/o). Increasing concentrations of aSPB or aSPC showed a highly significant reduction of lateral particle motility in

both protocols (Fig. 8D (protocol B) and Fig. S2 (protocol A)). Furthermore, combined application of both ABs leads to a further reduction of LBPs velocity close to zero (Fig. 8D and S2). As we expected, AB induced inactivation of the unpacking of LBPs resulted in a significant decline in lateral velocity, most likely due to the lack of insertion of surface active material into the A_{LI}. During ongoing LBP adsorption, γ typically falls from ~70 to ~30 mN/m (Bertocchi et al., 2005) causing different driving forces for LBP disintegration. To study the AB effects at a high γ, we analyzed particle velocity at the initial adsorption events (<30 sec). The results (Fig. 8E) showed no blocking effect at low individual AB concentrations but still a dramatic, even synergistic effect at combined AB application. This result could indicate that the function of each individual protein is less prominent at high γ, but an absolute requirement at those low γ values that normally exist in the lung (~ 30 mN/m (Schurch et al., 1976)). It therefore seems that interplay between both proteins is especially essential to reach highest material insertion (i.e. highest surface pressure) under moderate γ (low driving forces).

Summary and Conclusion

In summary, blocking SP-C and SP-B on the surface of freshly released LBPs dramatically disrupts their functionality at an A_{LI}, demonstrated by the absence of formation of surface films concomitant with an accumulation of unexpanded LBPs. This finding eventually provides the molecular mechanism for the interpretation of *in vivo* experiments conducted as early as twenty years ago. In these studies, it has been shown that application of aSPB into the lungs of healthy rabbits and mice lead to a lethal respiratory failure as early as 15 min after intratracheal instillation. Specifically, it has been shown that blocking SP-B lead to disease syndromes similar to those seen in the course of ARDS associated with striking fall in lung-thorax compliance, vastly elevated minimum γ and to a massively retarded surfactant adsorption combined with alveolar collapse. These severe pathological and histological effects were only observed in aSPB treated animals but not in the IgG control groups, disclosing an immunological effect (Fujita et al., 1988). Suzuki et al. and Fujita et al. reported an accumulation of "unexpanded lamellar bodies" in the alveolar lining fluid and suggested an interference with their normal ability to transform into a surface active film (Fujita et al., 1988;Suzuki et al., 1988). These lamellar bodies also contained an electron dense material which obviously did not disintegrate in the alveolar fluid. Importantly, though, none of these early studies and, to our knowledge not even up to now, attempted to test for an aSPC effect although the important role of this protein in surfactant film formation has long been known.

Here, we show that the hydrophobic surfactant proteins SP-B and SP-C are not only enclosed in intracellular surfactant (LBs) but also exposed in the release particles (LBPs). SP-B and SP-C localization is evidenced by immunofluorescence of extruding LBPs and by the strong effect of ABs on their adsorptive capacity at an A_{LI}. We hypothesize that these proteins are forming large hydrophobic pores that interact with, or that are target of, the forces acting at an A_{LI}. The recent structure reported for a large SP-B ring-shaped oligomer supports such a concept (Olmeda et al., 2015). Although the kind of action affecting the interfacial behavior of SP-B oligomer is obscure, we propose the following possible models: SP-B-based ring-shaped oligomers could be located at the outermost surfactant layer in LBPs, which previously to exocytosis could be in contact with the LB limiting membrane, where the ATP-driven ABCa3 pump is in charge of importing surface active lipids (Perez-Gil, 2008;Yamano et al., 2001). The progressive action of ABCa3 during LB biogenesis could accumulate lipids to generate a highly packed "energized" state with particular order and hydration properties that have been recently described (Cerrada et al., 2015) (see model in Fig. 9). Upon secretion, the highly packed activated state is preserved (Cerrada et al., 2015) enclosed into the now limiting membrane of LBPs, where SP-B/SP-C structures are exposed to the

extracellular environment. The eventual contact of SP-B machinery, at the surface of secreted LBPs, with the A_{LI} could trigger a conformational transition opening, or disassembling, the ring, which would then liberate a rapid flow of surface active lipids into the interface, possibly facilitated by the sudden liberation of the high internal pressure of LBPs, generated by the primary action of ABCa3 but maintained by a closed conformation of the SP-B ring. Binding of aSPB antibodies to those SP-B-triggered LBP surface machineries could block the surface-activated opening mechanism and prevent LBP spreading (see Fig. 9, right panel). The machinery could be also blocked by aSPC antibodies, if SP-C could also take part in the SP-B gating structure. We have determined that SP-C reduces the size of pores created in membranes by SP-B (Parra et al., 2013), which could be indicative of a direct SP-B/SP-C contact. The combined effect of aSPB and aSPC antibodies to block LBP interfacial adsorption could mean that the gating machinery exposes both SP-B and SP-C epitopes, either simultaneous or sequentially, and that the possibility of blockage at both sites increases the inhibitory capacities of combined antibodies. Irrespective of the real molecular mode of action, which should still be investigated, the hydrophobic surfactant proteins B and C have a combined essential role in the unpacking of the large LBPs and in promoting a rapid delivery and a bulk transfer of surface active materials onto an A_{LI}. Disturbances in this process may well explain the inhibitory effect of some substances (cholesterol, meconium, serum components etc. (William et al., 1999)) but also the dramatic pulmonary consequences that has been documented by former in-vivo animal experiments.

Materials and methods

Reagents

Unless otherwise specified, all reagents have been purchased from Sigma (Germany) and Life Technologies (Germany). Elastase from porcine Pancreas for cell isolation was purchased from Elastin Product Company (US). For bath solution we used standard Ringer Solution containing (in mM): 140 NaCl, 5 KCl, 1 MgCl2, 2 CaCl2, 10 HEPES, pH 7.4. Rabbit mature anti-SPB (WRAB-48604) and rabbit mature anti-SPC (WRAB-76694) were purchased from Sevenhills Bioreagents (US). IgG (Cat. # 31235) from Life Technologies was used as neg. ctrl for the functional studies. Rabbit antibodies were protein A purified and concentrations were verified with an Easy-Titer™ rabbit IgG Assay Kit (Life Technologies, Germany). For the functional studies antibodies were further diluted into bath solution to assay dependent concentration.

Surfactant preparations and quantification

LBPs were harvested from the supernatants of purified rat AT II cells grown on petri dishes (Ø 10 cm) in high density. AT II cells were isolated from Sprague-Dawley rats as described elsewhere (Haller et al., 1998). After two days in culture, these cells were washed two times with PBS and cells were stimulated for 4 h at 37 °C in 4 ml bath solution containing ATP (100 µM), PMA (300 nM) and Ionomycin (1 µM) supplemented with antibiotics as previously described. After stimulation, supernatants containing exocytosed surfactant rich in LBPs were collected filtered and stored at -20 °C until use. Subsequently phospholipid concentration of collected LBPs was measured by a lipid chloroform/methanol extraction protocol followed by choline determination using a coupled enzymatic reaction according to published references, with slight modifications, which are precisely explain in our recent publications (Hobi et al., 2014;Miklavc et al., 2012;Ravasio et al., 2008).

Fixed cell immunofluorescence

For immunofluorescence staining, ATII cells after isolation were seeded on 8-well ibidi dishes (IBIDI Gmbh, Germany). After two days cells, were washed twice in prewarm PBS (pH 7.4, Biochrom, Berlin, Germany), subsequently fixed for 20 minutes in 4% paraformaldehyde in PBS and permeabilized for 10 minutes with 0.2% saponin and 10% FBS (Thermo Scientific, Bonn, Germany) in PBS. Cells were subsequently stained for 30 min on room temperature with 1:300 diluted primary antibodies (mouseABCa3 (Abcam ac24751), rabbit aSPB (WRAB-76694), rabbit aSPC (WRAB-48604)) in PBS, 0.2% saponin and 10% FBS. Followed by four times washing with PBS and incubation with 1:500 diluted secondary antibody goat anti-mouse-Alexa568 (Life Technologies) and goat anti-rabbit-Alexa488 (Life Technologies) and 0.5 µg/ml Hoechst 33342 in in PBS, 0.2% saponin and 10% FBS. Unspecific binding of was precluded by direct application of secondary-Alexa antibodies. Images were taken on an inverted confocal microscope (Leica TCS SP5, Leica, Germany) using a 63× lens (Leica HCX PL APO lambda blue 63.0× 1.40 NA Oil UV). Several z-stack images for the blue (Hoechst 350), green (Alexa Fluor 488), red (Alexa Fluor 568) channels were taken in sequential mode using appropriate excitation and emission settings. Further image to montage processing was done in Fiji (NIH, United States) and final figure processing in Adobe Photoshop.

Electrophoresis and Western blot

For electrophoresis testing LBPs and rat bronchial lavage (BAL) samples were concentrated by ultracentrifugation (Ravasio et al., 2010). SDS/PAGE was performed under non reducing conditions in 16% acrylamide gels. Transfer of proteins to PVDF membranes (Bio-Rad, Spain) was performed

in a wet transfer system at 300 mA for 1 hour. 32µg total phospholipid mass was loaded in to the gel for detecting SP-B and 16µg for SP-C. Primary antibodies from Sevenhills (US) were diluted to 1:3000 for aSPB and 1:7000 for aSPC. Secondary antibody swine anti rabbit HRP-conjugated from Dako (Denmark) was diluted to 1:10000. Blot were analyzed in the ImageQuant LAS 4000 device (GE Healthcare, Germany) and further processed in Fiji and Adobe Photoshop.

Life cell Immunofluorescence

ATII cells were seeded in 8-well ibidi dishes (*Ibidi* GmbH, Germany) and used for experiments 2 days after isolation. Cells were stimulated with 100µm ATP for 15 min at 37°C. All stainings were done on living cells, under cold conditions to prevent unspecific binding or intracellular AB uptake by endocytosis, without using fixation or permeabilization buffers. Subsequently cells were kindly washed two-times with ice-cold bath solution, followed by incubation with 1:100 rabbit aSPB and aSPC in bath solution for 30 min at 4°C. Afterwards cells were again kindly washed four times with ice cold bath solution. Further incubation with secondary donkey anti-rabbit Alexa488 antibody from Life Technologies was followed by careful 4 times washing step with bath solution. Images were taken under the iMic microscope (Till Photonics, Germany) with a 60x 1.35 NA Oil objective and appropriate filter set. Firstly, one movie was made for 2 min by making a snapshot in brightfield light (BF) and fluorescence light (excitation wavelength 488) every 3 seconds. After the first image acquisition FM1-43 was added to the bath solution (end concentration 1µM), which indicates substantially fused LBPs. Another image acquisition for FM1-43 fluorescence staining was taken for 2 min. Further Image to Montage and movie processing were done in Fiji (NIH, Bethesda, United States) and final figure processing in Adobe Photoshop.

Electron Scanning Microscopy

Freshly isolated AT II cells were seeded on glow discharged, carbon treated and 4h fibronectin coated sapphire discs (3 mm in diameter, 160 µm thick, Engineering Office M. Wohlwend GmbH, Sennwald, Switzerland). After two days cell were gently washed two times with warm bath solution and subsequently stimulated with 100µM ATP and 300nM PMA for 15 min at 37°C.Primary antibodies rabbit aSPB or aSPC were diluted 1:100 in PBS, incubated at 4°C for 45 min and subsequently AB was carefully washed out with repeated washing steps. Afterwards, secondary 25nm-goldlabeled anti rabbit-AB (Aurion, Netherland) was diluted 1:50 in PBS + 0,1% FCS and applied for 30 min, followed by gentle washing steps. After fixation with 2.5 % glutaraldehyde (in PBS, phosphate buffer and 1% saccharose) for several hours at room temperature the samples were dehydrated in increasing concentrations of propanol and then critical point dried with carbon dioxide

as translation medium (Critical Point Dryer CPD 030, BalTec, Principality of Liechtenstein). Finally, the cells were coated with 7 to 10 nm of carbon using a Baf 300 (BalTec, Principality of Liechtenstein). Samples were observed on a FE-SEM (Hitachi S-2500) operated at 10 kV acceleration voltage. Immuno-gold particles were visualized with backscattered electrons, surfaces with the secondary electron signal (Walther and Mueller M, 1985).

Microplate reader based adsorption Assay

BODIPY-PC was dissolved in DMSO to yield a concentration of 1 mg/ml. LBPs were stained by incubation with BODIPY-PC at 37 °C for 2h to obtain a final molar ratio of 4% (dye/surfactant) (Ravasio et al., 2008). Experiments were performed using an assay system specifically designed to evaluate interfacial adsorption of LBPs. It provides a direct readout of the amount of surfactant reaching the interface but also of the material, which stably associates with the forming interfacial film. This method is described in detail in a previous publication (Danhaive et al., 2015;Hobi et al., 2014;Ravasio et al., 2008). Briefly, the wells of a 96-well microplate (sterile, flat, transparent Cat.# 655185, Greiner, Germany) were filled with 100 µl of a solution containing 5 mg/ml Brilliant Black as a photoquencher. The plate was inserted into the microplate reader (TECAN GENios Plus, Switzerland) and all measurements with following standard settings: fluorescence top reading mode number of (485 ± 9 nm excitation and 540 ± 9 nm emission), flashes 3, lag time 0 µs, and integrations time 1000 µs. Firstly, unspecific effects of antibody solution (aSPB, aSPC, aIgG) were tested by measuring 4% BODIPY-PC loaded LBPs in the respective transparent bath solution (Fig. S1, Inlet). Secondly, one background measurement (Brilliant Black only), was obtained. Thirdly, the 96-well plate was moved out and 0.5 µg of 4% BODIPY-PC (dye/surfactant) labeled surfactant was injected into the bulk solution of the wells. Thereafter, a kinetic cycle of fluorescence measurements was started for one hour (cycle time = 1 min, orbital shaking = 30 s). Fluorescently labeled surfactant distributed within the well by orbital shaking, and was finally irreversibly adsorbed into the A_{LI}, where the fluorescence signal was detected and quantified kinetically. Data were normalized with respect to the transparent values and by subtracting the background. For illustration of the kinetic curve *(=kinetics)* we defined the maximum fluorescence value, which reflects steady state surfactant film formation after maximal adsorption as *Max* (Fig. S1) and the initial adsorption events are reflected as *Slope (*Fig. S1*).* Microsoft Excel and GraphPad Prism were used for background correction, student's t-test analyzing, *Max* and *Slope* calculation, and the final graph design.

Life cell inverted interface setup

For the microscopic experiments, we used our inverted interface setup, slightly modified for the needs of the experimental requirements (Hobi et al., 2012;Ravasio et al., 2010). The chamber is made of stainless steel (material description: 1.4542), which is highly resistant to corrosion, heat and acidity. The bottom is covered with a nanocoating, made of a glass-ceramic polar Si-O network with emedded nano-particles to avoid wetting of the chamber bottom. These special characteristics are important to establish a clean interface, which is kept in the 200µm capillary (=approx. same area as an alveolus) by adhesion and surface tension (Hobi et al., 2012;Ravasio et al., 2011)).

As shown in the sketch of Fig. 6, heated chamber was prefilled with warm Ringer solution and then LBPs pre-loaded with 6µM FM1-43 (3.6µg/ml) were gently pipette in the chamber. LBPs sediment due to gravity forces and upon interface contact they disintegrate. These dynamic adsorption events were imaged over time, under the inverted microscope (Axiovert from Zeiss equipped with a 40x LD-Achroplan, NA 0.6 air objective from Zeiss, and a cooled CCD camera, controlled by TiLLVison software, (Ravasio et al., 2011)). Timeseries were performed over 10 min with a snapshot each 5 seconds using fluorescence light with an excitation wavelength 488 nm, and appropriate filter set. Two different protocols were established for the AB application. In the first protocol FM1-43 stained LBPs were pipetted into chamber, prefilled with warm Ringer solution containing different concentrations of AB (2-100nM; direct antibody treatment= Protocol A). In a second protocol, LBPs were preincubated with AB solution (10nM-1µM) for 2 h, followed by gentle centrifugation steps (800g) for washing out the unbounded AB (preincubation antibody treatment= Protocol B). In initial studies we used respective IgG Fab fragments (Pierce™ Fab Preparation Kit, Thermo Scientific, Germany) to preclude any antibody self-assembly. Afterwards, LBPs were loaded with 6 µM FM1-43 and pipetted into chamber containing Ringer solution and timeseries acquisition was started. The total number of transformed LBPs was determined by manual evaluation in ImageJ. Further data analysis and column graph design were performed in Microsoft Excel and GraphPad Prism.

LBPs velocity

To determine the two dimensional movement distance and the average velocity of LBPs on the liquid surface the ETHZ MOSAIC Particle Tracker 2D/3D plugin for ImageJ (http://www.mosaic.ethz.ch/Downloads/ParticleTracker, (Sbalzarini and Koumoutsakos, 2005)) was used with following standard settings: Radius 3, Cutoff 3.0 and Per/Abs 0.1. Particle detection efficiency of the plugin was verified manually for every data set and for each movie 10 tracks were extracted into MS Excel for further processing. The robust plugin automatically records X and Y

values from tracked particle in each image. X and Y data were exported into MS Excl. The covered pixel distance of a particle between two time frames was analysed as followed:

$x = [\sqrt{\Delta x^2 + \Delta y^2}]$. The total velocity for initial adsorption (<30 sec) and over 10 min were calculated by summation of the single frame distances and pixel were converted to µm. LBPs velocity over 10 min of different conditions were compared to neg. ctrl (w/o).

Statistics

Image analysis and data presentation

Images were analyzed using iMic Online Analysis and Tillvision (Till Photonics, Germany), Fiji (NIH, Bethesda, United States). Microsoft Excel and GraphPad Prism 5 were used for *Max* and *Slope* calculations, background correction, statistics, and graph design. All data are presented as mean ± SEM with following *P* value assignments: Asterisk (*) was used to indicate significance against the corresponding control conditions (aIgG and w/o) *P**<0.05, *P***<0.01, *P****<0.001) and $P^{\#}$<0.05, $P^{\#\#}$<0.01, $P^{\#\#\#}$<0.001 if combined application of both ABs was significantly different to aSPB or aSPC alone in the respective concentration.

Acknowledgements

We thank T. Felder, I. Öttl, A. Riecker and G. Sieber, for technical assistance in particular for the isolation of primary alveolar type II cells, LBPs collection and assistance with the cell culture. This work was supported by grants of the Bausteinprogramm University of Ulm L.SBN.0103 (to N.H.) and grants from Spanish Ministry of Economy (BIO2012-30733) and the Regional Government of Madrid (S2013/MlT-2807) (to J. P.-G. and B. O.). Nina Hobi is supported by the Carl Zeiss Foundation.

Contributions

N.H, T.H. and J.PG. designed the study. P.D, E.F., M.F, M.G., N.H., T.H., P.M., B.O., P.W. performed experiments and analyzed data. N.H., T.H. and J.PG. wrote the manuscript.

Competing financial interests

The authors declare no competing financial interests.

References

Almlen, A., G.Stichtenoth, B.Linderholm, M.Haegerstrand-Bjorkman, B.Robertson, J.Johansson, and T.Curstedt. 2008. Surfactant proteins B and C are both necessary for alveolar stability at end expiration in premature rabbits with respiratory distress syndrome. *J. Appl. Physiol (1985.)* 104:1101-1108.

Bastacky, J., C.Y.Lee, J.Goerke, H.Koushafar, D.Yager, L.Kenaga, T.P.Speed, Y.Chen, and J.A.Clements. 1995. Alveolar lining layer is thin and continuous: low-temperature scanning electron microscopy of rat lung. *J Appl Physiol* 79:1615-1628.

Bernardino, d.l.S., R.Vargas, V.Picardi, A.Cruz, R.Arranz, J.M.Valpuesta, L.Mateu, and J.Perez-Gil. 2013. Segregated ordered lipid phases and protein-promoted membrane cohesivity are required for pulmonary surfactant films to stabilize and protect the respiratory surface. *Faraday Discuss.* 161:535-548.

Bertocchi, C., A.Ravasio, S.Bernet, G.Putz, P.Dietl, and T.Haller. 2005. Optical measurement of surface tension in a miniaturized air-liquid interface and its application in lung physiology. *Biophys J* 89:1353-1361.

Brasch, F., G.Johnen, A.Winn-Brasch, S.H.Guttentag, A.Schmiedl, N.Kapp, Y.Suzuki, K.M.Muller, J.Richter, S.Hawgood, and M.Ochs. 2004. Surfactant protein B in type II pneumocytes and intra-alveolar surfactant forms of human lungs. *Am. J. Respir. Cell Mol. Biol.* 30:449-458.

Cabre, E.J., L.M.Loura, A.Fedorov, J.Perez-Gil, and M.Prieto. 2012. Topology and lipid selectivity of pulmonary surfactant protein SP-B in membranes: Answers from fluorescence. *Biochim. Biophys. Acta* 1818:1717-1725.

Cabre, E.J., J.Malmstrom, D.Sutherland, J.Perez-Gil, and D.E.Otzen. 2009. Surfactant protein SP-B strongly modifies surface collapse of phospholipid vesicles: insights from a quartz crystal microbalance with dissipation. *Biophys. J.* 97:768-776.

Casals, C. 2001. Role of surfactant protein A (SP-A)/lipid interactions for SP-A functions in the lung. *Pediatr. Pathol. Mol. Med.* 20:249-268.

Cerrada, A., T.Haller, A.Cruz, and J.Perez-Gil. 2015. Pneumocytes Assemble Lung Surfactant as Highly Packed/Dehydrated States with Optimal Surface Activity. *Biophys. J.* 109:2295-2306.

Clark, J.C., S.E.Wert, C.J.Bachurski, M.T.Stahlman, B.R.Stripp, T.E.Weaver, and J.A.Whitsett. 1995. Targeted disruption of the surfactant protein B gene disrupts surfactant homeostasis, causing respiratory failure in newborn mice. *Proc. Natl. Acad. Sci. U. S. A* 92:7794-7798.

Cruz, A., L.A.Worthman, A.G.Serrano, C.Casals, K.M.Keough, and J.Perez-Gil. 2000. Microstructure and dynamic surface properties of surfactant protein SP-B/dipalmitoylphosphatidylcholine interfacial films spread from lipid-protein bilayers. *Eur. Biophys. J.* 29:204-213.

Danhaive, O., C.Chapin, H.Horneman, P.E.Cogo, and P.L.Ballard. 2015. Surface film formation in vitro by infant and therapeutic surfactants: role of surfactant protein B. *Pediatr. Res.* 77:340-346.

Dietl, P., and T.Haller. 2005. Exocytosis of lung surfactant: From the secretory vesicle to the air-liquid interface. *Annu Rev Physiol* 67:595-621.

Frick, M., S.Eschertzhuber, T.Haller, N.Mair, and P.Dietl. 2001. Secretion in alveolar type II cells at the interface of constitutive and regulated exocytosis. *American Journal of Physiology-Lung Cellular and Molecular Physiology* 2001/10/06:306-315.

Fujita, Y., K.Kogishi, and Y.Suzuki. 1988. Pulmonary damage induced in mice by a monoclonal antibody to proteins associated with pig pulmonary surfactant. *Exp. Lung Res.* 14:247-260.

Gil, J., and O.K.Reiss. 1973. Isolation and characterization of lamellar bodies and tubular myelin from rat lung homogenates. *J. Cell Biol.* 58:152-171.

Glasser, S.W., M.S.Burhans, T.R.Korfhagen, C.L.Na, P.D.Sly, G.F.Ross, M.Ikegami, and J.A.Whitsett. 2001. Altered stability of pulmonary surfactant in SP-C-deficient mice. *Proc. Natl. Acad. Sci. U. S. A* 98:6366-6371.

Glasser, S.W., A.P.Senft, J.A.Whitsett, M.D.Maxfield, G.F.Ross, T.R.Richardson, D.R.Prows, Y.Xu, and T.R.Korfhagen. 2008. Macrophage dysfunction and susceptibility to pulmonary Pseudomonas aeruginosa infection in surfactant protein C-deficient mice. *J. Immunol.* 181:621-628.

Gross, N.J., and R.M.Schultz. 1990. Serine proteinase requirement for the extra-cellular metabolism of pulmonary surfactant. *Biochim. Biophys. Acta* 1044:222-230.

Haller, T., P.Dietl, K.Pfaller, M.Frick, N.Mair, M.Paulmichl, M.W.Hess, J.Furst, and K.Maly. 2001. Fusion pore expansion is a slow, discontinuous, and Ca2+-dependent process regulating secretion from alveolar type II cells. *J Cell Biol* 155:279-289.

Haller, T., P.Dietl, H.Stockner, M.Frick, N.Mair, I.Tinhofer, A.Ritsch, G.Enhorning, and G.Putz. 2004. Tracing surfactant transformation from cellular release to insertion into an air-liquid interface. *Am J Physiol Lung Cell Mol Physiol* 286:L1009-L1015.

Haller, T., J.Ortmayr, F.Friedrich, H.Volkl, and P.Dietl. 1998. Dynamics of surfactant release in alveolar type II cells. *Proc. Natl. Acad. Sci. U. S. A* 95:1579-1584.

Hawgood, S., M.Derrick, and F.Poulain. 1998. Structure and properties of surfactant protein B. *Biochim. Biophys. Acta* 1408:150-160.

Herting, E., X.Gan, P.Rauprich, C.Jarstrand, and B.Robertson. 1999. Combined treatment with surfactant and specific immunoglobulin reduces bacterial proliferation in experimental neonatal group B streptococcal pneumonia. *Am. J. Respir. Crit Care Med.* 159:1862-1867.

Hobi, N., A.Ravasio, and T.Haller. 2012. Interfacial stress affects rat alveolar type II cell signaling and gene expression. *American Journal of Physiology-Lung Cellular and Molecular Physiology* 303:L117-L129.

Hobi, N., G.Siber, V.Bouzas, A.Ravasio, J.Perez-Gil, and T.Haller. 2014. Physiological variables affecting surface film formation by native lamellar body-like pulmonary surfactant particles. *Biochim. Biophys. Acta* 1838:1842-1850.

Holm, B.A., R.H.Notter, and J.N.Finkelstein. 1985. Surface property changes from interactions of albumin with natural lung surfactant and extracted lung lipids. *Chem Phys Lipids.* 38:287-298.

Klenz, U., M.Saleem, M.C.Meyer, and H.J.Galla. 2008. Influence of lipid saturation grade and headgroup charge: A refined lung surfactant adsorption model. *Biophys J* 95:699-709.

Kliewer, M., E.K.Fram, A.R.Brody, and S.L.Young. 1985. Secretion of surfactant by rat alveolar type II cells: morphometric analysis and three-dimensional reconstruction. *Exp. Lung Res.* 9:351-361.

Lawson, W.E., V.V.Polosukhin, G.T.Stathopoulos, O.Zoia, W.Han, K.B.Lane, B.Li, E.F.Donnelly, G.E.Holburn, K.G.Lewis, R.D.Collins, W.M.Hull, S.W.Glasser, J.A.Whitsett, and T.S.Blackwell. 2005. Increased and prolonged pulmonary fibrosis in surfactant protein C-deficient mice following intratracheal bleomycin. *Am. J. Pathol.* 167:1267-1277.

Liou, W., H.J.Geuze, and J.W.Slot. 1996. Improving structural integrity of cryosections for immunogold labeling. *Histochem. Cell Biol.* 106:41-58.

Lukovic, D., A.Cruz, A.Gonzalez-Horta, A.Almlen, T.Curstedt, I.Mingarro, and J.Perez-Gil. 2012. Interfacial behavior of recombinant forms of human pulmonary surfactant protein SP-C. *Langmuir* 28:7811-7825.

Mahler, H.C., F.Senner, K.Maeder, and R.Mueller. 2009. Surface activity of a monoclonal antibody. *J. Pharm. Sci.* 98:4525-4533.

Melton, K.R., L.L.Nesslein, M.Ikegami, J.W.Tichelaar, J.C.Clark, J.A.Whitsett, and T.E.Weaver. 2003. SP-B deficiency causes respiratory failure in adult mice. *Am. J. Physiol Lung Cell Mol. Physiol* 285:L543-L549.

Miklavc, P., E.Hecht, N.Hobi, O.H.Wittekindt, P.Dietl, C.Kranz, and M.Frick. 2012. Actin coating and compression of fused secretory vesicles are essential for surfactant secretion - a role for Rho, formins and myosin II. *Journal of Cell Science* 125:2765-2774.

Ochs, M. 2010. The Closer we Look the more we See? Quantitative Microscopic Analysis of the Pulmonary Surfactant System. *Cellular Physiology and Biochemistry* 25:27-40.

Olmeda, B., B.Garcia-Alvarez, M.J.Gomez, M.Martinez-Calle, A.Cruz, and J.Perez-Gil. 2015. A model for the structure and mechanism of action of pulmonary surfactant protein B. *FASEB J.* 29:4236-4247.

Parra, E., A.Alcaraz, A.Cruz, V.M.Aguilella, and J.Perez-Gil. 2013. Hydrophobic Pulmonary Surfactant Proteins SP-B and SP-C Induce Pore Formation in Planar Lipid Membranes: Evidence for Proteolipid Pores. *Biophys J* 104:146-155.

Parra, E., and J.Perez-Gil. 2015. Composition, structure and mechanical properties define performance of pulmonary surfactant membranes and films. *Chem. Phys. Lipids* 185:153-175.

Pastrana, B., A.J.Mautone, and R.Mendelsohn. 1991. Fourier transform infrared studies of secondary structure and orientation of pulmonary surfactant SP-C and its effect on the dynamic surface properties of phospholipids. *Biochemistry* 30:10058-10064.

Perez-Gil, J. 2008. Structure of pulmonary surfactant membranes and films: The role of proteins and lipid-protein interactions. *Biochim Biophys Acta* 1778:1676-1695.

Perez-Gil, J., C.Casals, and D.Marsh. 1995. Interactions of hydrophobic lung surfactant proteins SP-B and SP-C with dipalmitoylphosphatidylcholine and dipalmitoylphosphatidylglycerol bilayers studied by electron spin resonance spectroscopy. *Biochemistry* 34:3964-3971.

Plasencia, I., A.Cruz, C.Casals, and J.Perez-Gil. 2001. Superficial disposition of the N-terminal region of the surfactant protein SP-C and the absence of specific SP-B-SP-C interactions in phospholipid bilayers. *Biochem. J.* 359:651-659.

Ravasio, A., A.Cruz, J.Perez-Gil, and T.Haller. 2008. High-throughput evaluation of pulmonary surfactant adsorption and surface film formation. *J Lipid Res* 49:2479-2488.

Ravasio, A., N.Hobi, C.Bertocchi, A.Jesacher, P.Dietl, and T.Haller. 2011. Interfacial sensing by alveolar type II cells: a new concept in lung physiology? *American Journal of Physiology-Cell Physiology* 300:C1456-C1465.

Ravasio, A., B.Olmeda, C.Bertocchi, T.Haller, and J.Perez-Gil. 2010. Lamellar Bodies Form Solid Three-dimensional Films at the Respiratory Air-Liquid Interface. *J Biol Chem* 285:28174-28182.

Roldan, N., E.Goormaghtigh, J.Perez-Gil, and B.Garcia-Alvarez. 2015. Palmitoylation as a key factor to modulate SP-C-lipid interactions in lung surfactant membrane multilayers. *Biochim. Biophys. Acta* 1848:184-191.

Sbalzarini, I.F., and P.Koumoutsakos. 2005. Feature point tracking and trajectory analysis for video imaging in cell biology. *J. Struct. Biol.* 151:182-195.

Schürch, D., O.L.Ospina, A.Cruz, and J.Perez-Gil. 2010. Combined and Independent Action of Proteins SP-B and SP-C in the Surface Behavior and Mechanical Stability of Pulmonary Surfactant Films. *Biophys J* 99:3290-3299.

Schurch, S., J.Goerke, and J.A.Clements. 1976. Direct determination of surface tension in the lung. *Proc. Natl. Acad. Sci. U. S. A* 73:4698-4702.

Serrano, A.G., and J.Perez-Gil. 2006. Protein-lipid interactions and surface activity in the pulmonary surfactant system. *Chemistry and Physics of Lipids* 141:105-118.

Singer, W., M.Frick, T.Haller, S.Bernet, M.Ritsch-Marte, and P.Dietl. 2003. Mechanical forces impeding exocytotic surfactant release revealed by optical tweezers. *Biophys. J.* 84:1344-1351.

Stahlman, M.T., M.P.Gray, M.W.Falconieri, J.A.Whitsett, and T.E.Weaver. 2000. Lamellar body formation in normal and surfactant protein B-deficient fetal mice. *Lab Invest* 80:395-403.

Suzuki, Y., B.Robertson, Y.Fujita, and G.Grossmann. 1988. Respiratory failure in mice caused by a hybridoma making antibodies to the 15 kDa surfactant apoprotein. *Acta Anaesthesiol Scand* 32:283-289.

Taeusch, H.W., J.B.de la Serna, J.Perez-Gil, C.Alonso, and J.A.Zasadzinski. 2005. Inactivation of pulmonary surfactant due to serum-inhibited adsorption and reversal by hydrophilic polymers: Experimental. *Biophys J* 89:1769-1779.

Tokieda, K., J.A.Whitsett, J.C.Clark, T.E.Weaver, K.Ikeda, K.B.McConnell, A.H.Jobe, M.Ikegami, and H.S.Iwamoto. 1997. Pulmonary dysfunction in neonatal SP-B-deficient mice. *Am. J. Physiol* 273:L875-L882.

Vandenbussche, G., A.Clercx, T.Curstedt, J.Johansson, H.Jornvall, and J.M.Ruysschaert. 1992. Structure and orientation of the surfactant-associated protein C in a lipid bilayer. *Eur. J. Biochem.* 203:201-209.

Walther, P., and Mueller M. 1985. Detection of small (5-15 nm) gold labelled surface antigens using backscattered electrons. *In* Science of Biological Specimen, Preparation. Mueller M., Becker RP., Boyde A., and Wolosewick JJ., editors. AMF O'Hare SEM, Chicago. 195-201.

Wang, Z., O.Gurel, J.E.Baatz, and R.H.Notter. 1996. Differential activity and lack of synergy of lung surfactant proteins SP-B and SP-C in interactions with phospholipids. *J. Lipid Res.* 37:1749-1760.

Weaver, T.E., and D.C.Beck. 1999. Use of knockout mice to study surfactant protein structure and function. *Biol. Neonate* 76 Suppl 1:15-18.

William, T.H., K.W.Lu, J.Goerke, and J.A.Clements. 1999. Nonionic polymers reverse inactivation of surfactant by meconium and other substances. *Am. J. Respir. Crit Care Med.* 159:1391-1395.

Yamano, G., H.Funahashi, O.Kawanami, L.X.Zhao, N.Ban, Y.Uchida, T.Morohoshi, J.Ogawa, S.Shioda, and N.Inagaki. 2001. ABCA3 is a lamellar body membrane protein in human lung alveolar type II cells. *FEBS Lett.* 508:221-225.

Zasadzinski, J.A., T.F.Alig, C.Alonso, J.B.de la Serna, J.Perez-Gil, and H.W.Taeusch. 2005. Inhibition of pulmonary surfactant adsorption by serum and the mechanisms of reversal by hydrophilic polymers: theory. *Biophys J.* 89:1621-1629.

Fig. 1

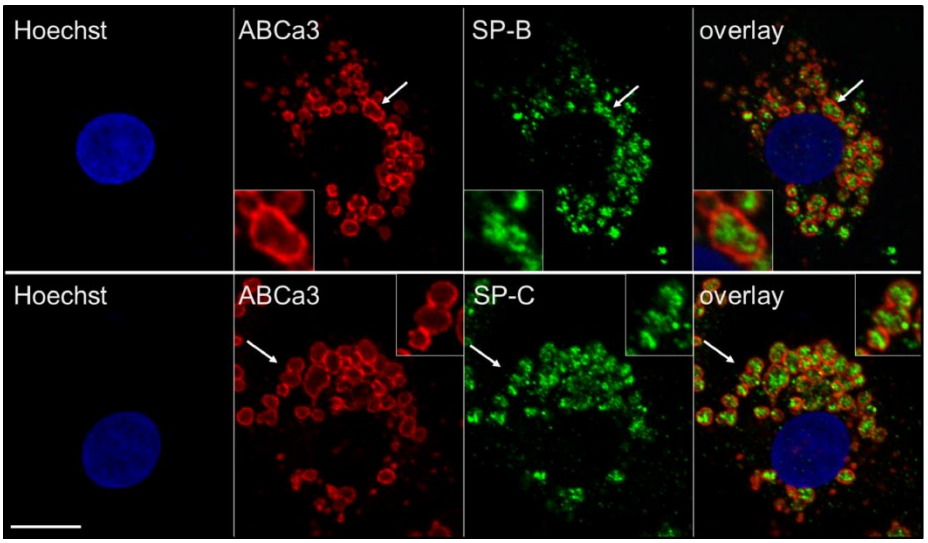

FIGURE1 **SP-B and SP-C are highly expressed in 48h cultured, primary ATII cells.** The red channel indicates the lamellar body (LB) specific marker ABCa3 and the green channel the expression of SP-B (upper row) and SP-C (lower row) within the lumen of LBs. Areas of enlargement are indicated by the arrows. Cells in this phenotypic state have been used for the collection of Lamellar Body-like Particles (LBPs), exocytosed by the ATII cells after agonist stimulation. Scale bar: 5 µm.

Fig. 2

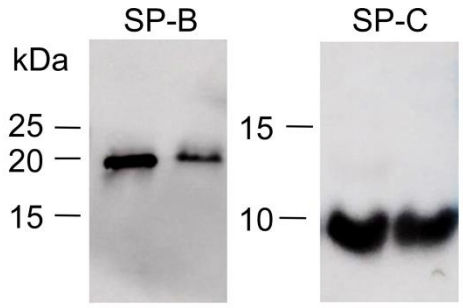

FIGURE2 **Freshly collected LBPs contain SP-B and SP-C.** Left: Under non-reducing conditions, samples (LBP) demonstrate a specific SP-B band with mobility corresponding to 18 kDa, indicative for a covalent SP-B dimer. A comparable band can be seen in rat bronchoalveolar lavage (BAL) serving as positive control. Right: Specific SP-C band in the test sample and in BAL positive control. Presented Western blots are representative for n=3.

Fig. 3

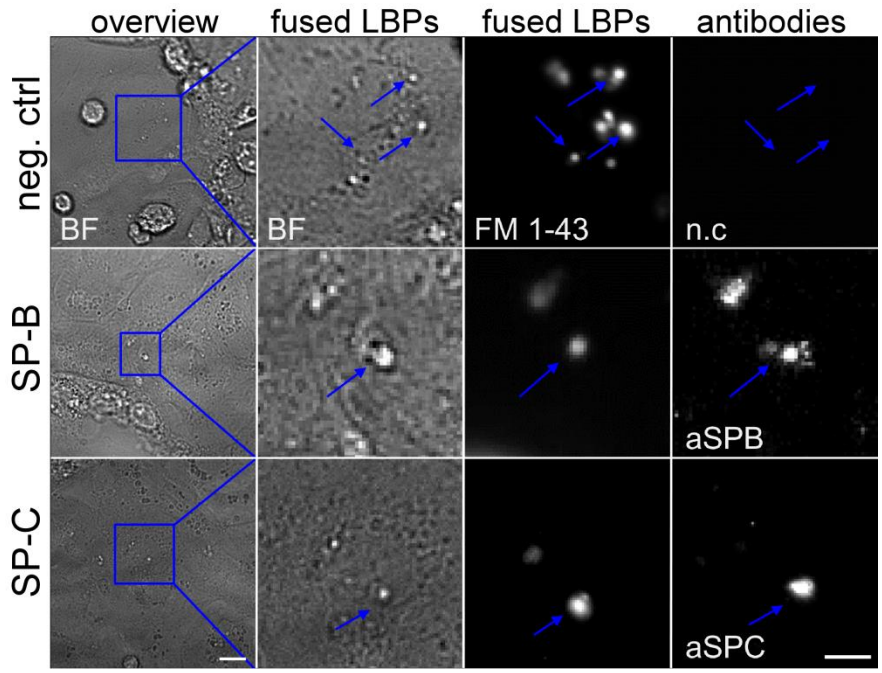

FIGURE3 **SP-B and SP-C are located on extracellular LBPs surface.** AII cells have been stimulated with ATP and subsequently stained with primary and secondary ABs. Fused vesicles release LBPs as protrusions (arrows) out of the cell membrane, seen in brightfield (BF) and by extracellular application of FM1-43, a lipid membrane fluorescent probe not penetrating intact membranes (FM 1-43). All stainings have been performed in living cells without using fixation or permeation buffer at 4° C. Negative controls (n.c.; Movie S1) without aSPB or aSPC (upper panel) precludes unspecific AB binding. Specific signals were obtained with primary AB (aSPB, aSPC; Movies S2 and S3). Images are representative for n=5. Scale bar: 10 µm.

Fig. 4

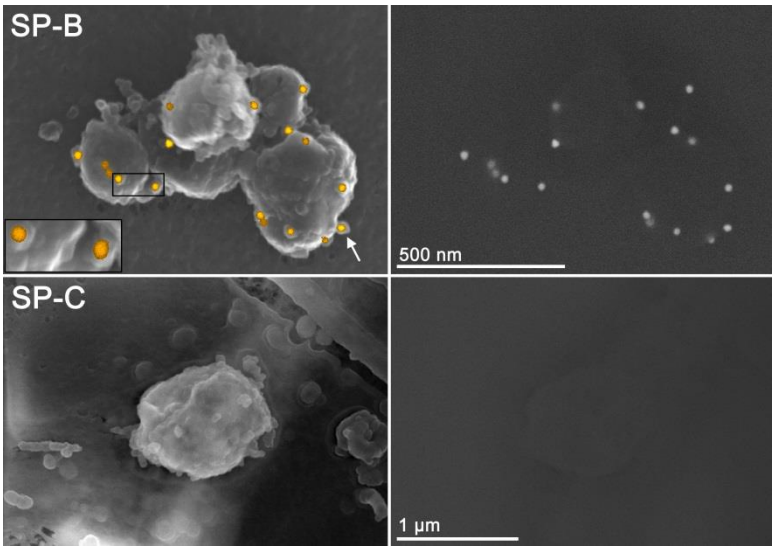

FIGURE4 **SEM of cell attached LBPs**. Scanning electron microscopy of stimulated ATII cells show LBPs as ballon-like protrusions out of the plain of the cell membrane. Immunogold label for SP-B was specific (top, right) and co-localizes predominantly to wart-like surface structures on the outermost LBP membranes (top left, inset and arrow). SP-C was not detectable (bottom, left and right).

Fig. 5

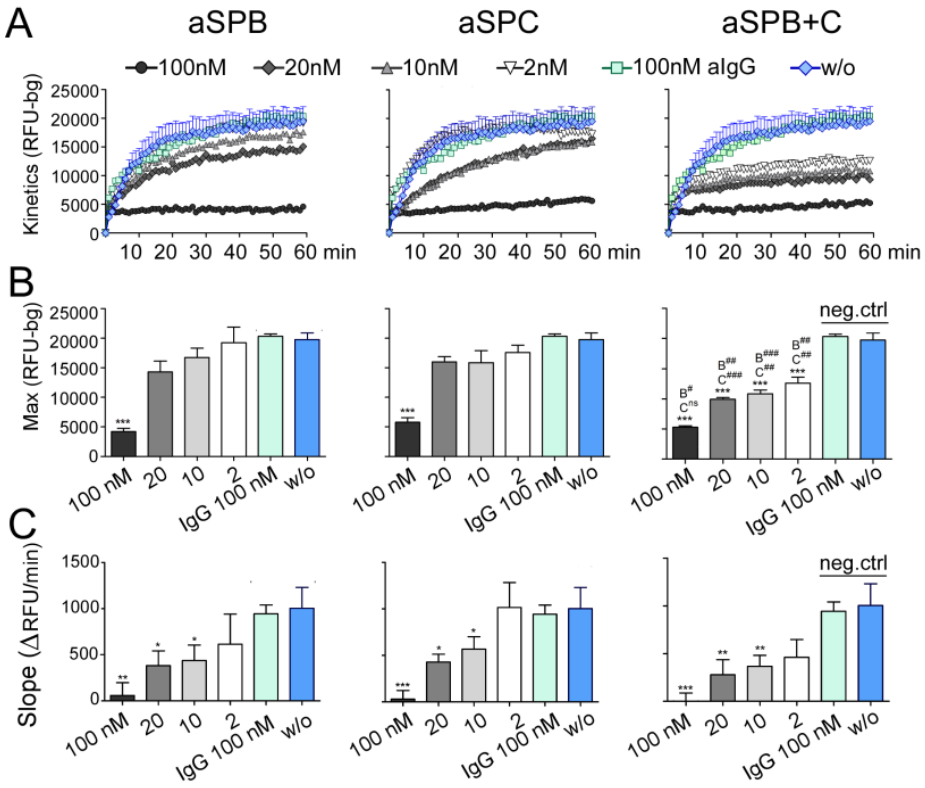

FIGURE5 **Adsorption Assay of fluorescently labeled LBPs.** LBPs were treated with aSPB or aSPC (2nM-100nM) separately or in a 1/1 combination (aSPB+C=2nM-100nM). Bath solution (w/o) and 100nM aIgG served as negative controls. A: Adsorption kinetics. 100nM aSPB or aSPC had a dramatic effect on LBP adsorption (= surface film formation; n=6; Error bars, except for the w/o groups, have been omitted for better visibility). B: Maximum Adsorption (*Max*). We defined *Max* as the values obtained between 57-60 min from the tracings in panel A (Fig. S1). Both surfactant proteins are important for reaching *Max*. Combined application of both ABs (n= 10-14) lead to a summative effect and significantly blocked *Max* adsorption. C: Rate of initial adsorption (*Slope).* *Slope* was calculated between 2-6 min from the tracings in panel A (Fig. S1). Both AB applications decreased the adsorption kinetics at initial stages; however there was no additive effect when applied in combination. Significant differences against w/o are indicated by asterisks (*P**<0.05, *P***<0.01, *P****<0.001). Significant differences of combined application (aSPB+C) versus aSPB or aSPC are indicated with hashtags against SP-B (B#) and SP-C (C#), respectively (*P*#<0.05, *P*##<0.01, *P*###<0.001). RFU-bg: relative fluorescence units with subtracted background.

Fig. 6

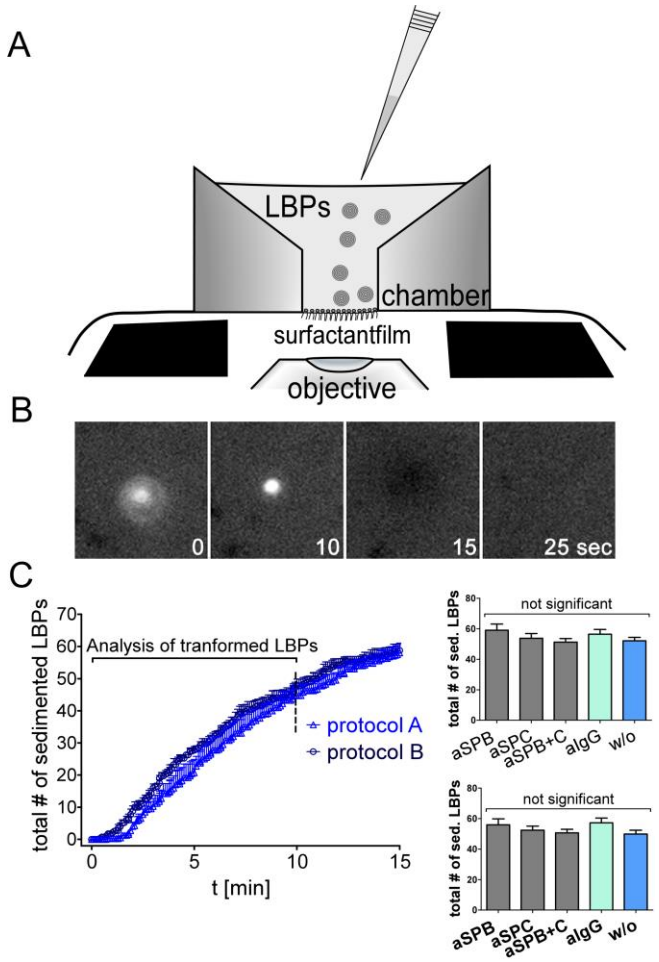

FIGURE6 **Interfacial transfer of LBPs at the inverted interface experiments.** A: Sketch of the microscopic setup. The thermostated chamber, filled with bath solution, is placed over a 40× LD objective. FM1-43 loaded LBPs were added on top. Thereupon adsorption dynamics was captured in a time lapse mode over 10 min. In protocol A the bath solution contained different AB concentrations. In protocol B, LBPs were pre-incubated with AB for 2h followed by a washout of unbound AB before addition to the chamber. B: Time resolved image series showing the arrival (0 to 10 sec) and the subsequent adsorption (15 to 25 sec) of a single FM 1-43 loaded LBP at the inverted interface (Movie S4A and S4B). Image size 130x130 pixel. C: Left: Analysis of LBP adsorption. The representative tracings (n=4) show the cumulative count of LBPs arriving at the interface using protocol A or B. Right: Within the analyzed time (10 min), the number of sedimented LBPs was similar in both approaches (50±2 for w/o protocol A and 52±2 for w/o protocol B). AB treatment did not affect LBP sedimentation (n=20). Upper graph: protocol A, lower graph: protocol B.

Fig. 7

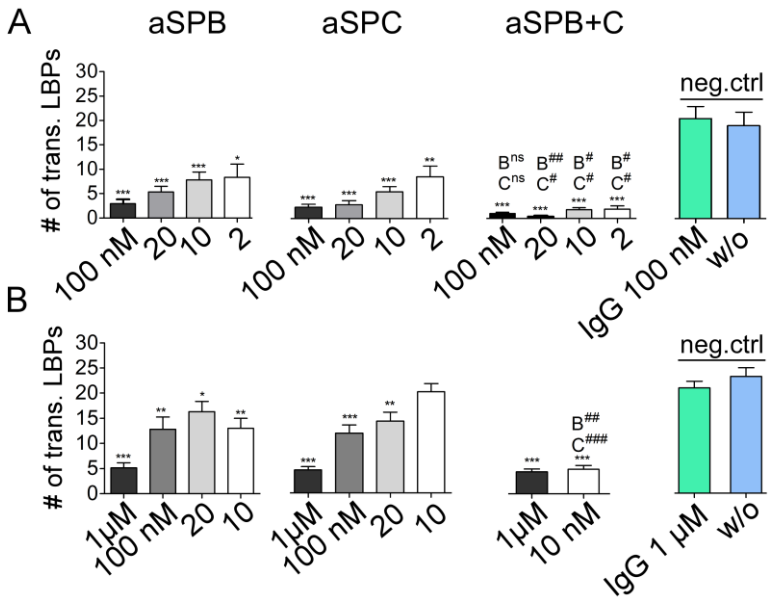

FIGURE7 **Blockage of LBPs adsorption**. A: In protocol A, application of aSPB or aSPC in all concentrations showed a strong significant reduction of LBPs transformation. The combined application of aSPB and aSPC (aSPB+C) lead to a further specific reduction in comparison to individual AB application. B: In protocol B, application of aSPB lead to a significant inhibition of particle transformation at all concentrations. aSPC had significant effects at concentrations >10nM. Significant difference against w/o is indicated with asterisks *P**<0.05, *P***<0.01, *P****<0.001 and against single application of aSPB or aSPC with hashtags *P*#<0.05, *P*##<0.01, *P*###<0.001 against aSPB and aSPC (n=10-15).

Fig. 8

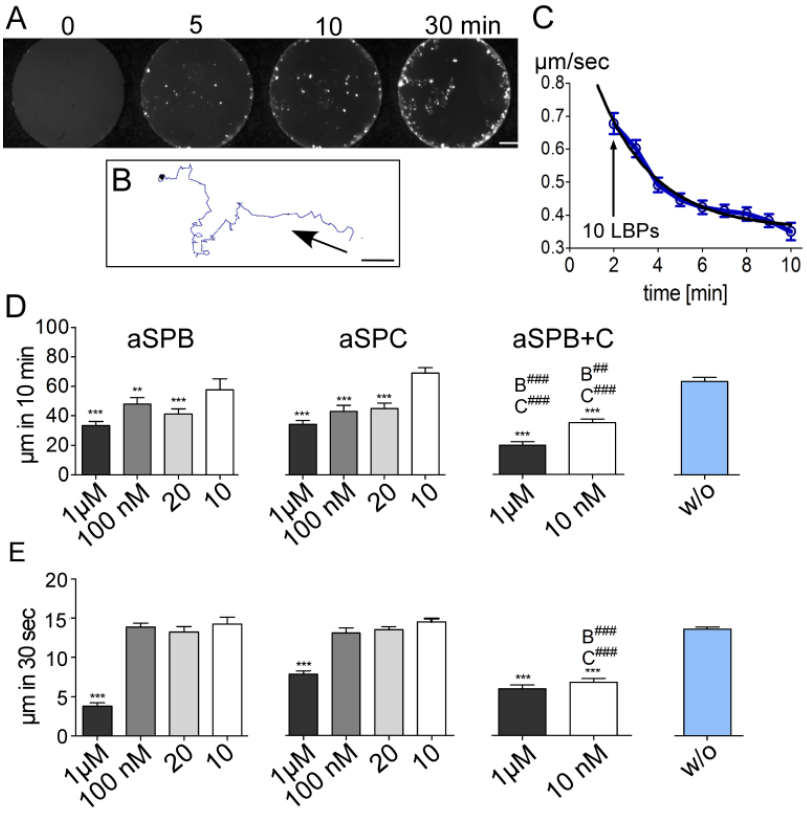

FIGURE8 **LBPs velocity at the interface**: A: Time-lapse of adsorbing LBPs at the A_{LI} over 30 min. At very early stages of the measurements, LBPs completely disintegrate (=disappear) upon A_{LI} contact due to a high γ (=clean A_{LI}). Subsequent LBPs adsorption is getting slower and incomplete, leaving behind smaller units amenable for analysis. Scale bar = 50 µm. Particles can be reliably recognized by using particle tracking plugin from MOSAIC plugin from ImageJ. The program detects spot-like surface structures of a defined cut-off for fluorescence intensity and pixel size B: Example of particle track over 10 min (Movie S5). Arrows indicate direction of particle. Scale bar = 5 µm. C: In control conditions particle velocity is highest at initial stages of adsorption due to high γ gradients. Curve describes decrease in particle velocity (µm/sec) as an exponential decay (Spearman's corr. coeffi. =-0.93; $P < 0.0001$, n=4 representative tracks). D: Particle velocity within the first 10 min in protocol B. Blocking SP-B or SP-C individually leads to a significant reduction of particle velocity (i.e surface pressure) in almost all concentrations. Combined application of aSPB and aSPC (aSPB+C) lead to a further reduction. E: Particle velocity at initial events (protocol B). Using aSPB or aSPC in lower concentration (10nM-100nM) did not inhibit velocity. Combined application of 10nM aSPB+C showed a synergetic effect on surfactant surface activity. Significant difference against w/o is indicated with asterisks P*<0.05, P**<0.01, P***<0.001 and combined

application versus single application of aSPB or aSPC is indicated with hashtags P#<0.05, P##<0.01, P###<0.001 against aSPB and aSPC (n=100-120).

Fig. 9

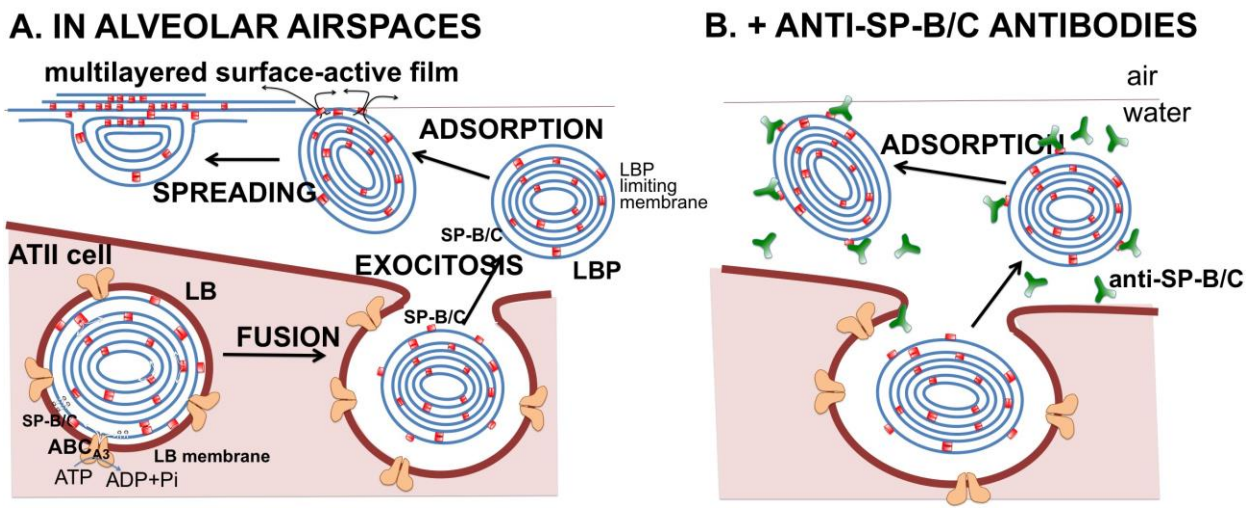

FIGURE9 **Model for SP-B/C dependent adsorption of LPBs and its blocking by antibodies**. A: ATP-driven pumping of surface active phospholipids by the ABCa3 protein of the LB limiting membrane is thought to generate the highly packed structure of lung surfactant stores in LBs. Upon secretion and associated to changes in the environment of LBs, a "closed state" of the SP-B-based machinery could be important to still maintain surfactant lipids in a highly packed state (=LBPs). When secreted LBPs contact with the A_{LI}, a conformational change occurring at the SP-B/C machinery could trigger its opening to gain access to the internal lipid content and liberate a rapid flow and transfer of surface active species. B: In the presence of anti-SP-B and/or anti-SP-C antibodies, the machinery controlling the protein "gates" at the surface of LBPs could be permanently blocked, preventing the spreading of surfactant lipids at the interface.